Chemical Sciences Journal
ISSN: 2150-3494

Rasheed et al., Chem Sci J 2018, 9:4
DOI: 10.4172/2150-3494.1000197

Research Article Open Access

Preparation and Characterization of Hematite Iron Oxide (α-Fe_2O_3) by Sol-Gel Method

Rasheed RT[1*], Al-Algawi SD[2], Kareem HH[3] and Mansoor HS[3]

[1]*Applied Chemistry Division, School of Applied Sciences, University of Technology, Baghdad, Iraq*

[2]*Applied Physics Division, School of Applied Sciences, University of Technology, Baghdad, Iraq*

[3]*Material Science Division, School of Applied Sciences, University of Technology, Baghdad, Iraq*

[*]**Corresponding author:** Rasheed RT, Applied Chemistry Division, School of Applied Sciences, University of Technology, Baghdad, Iraq, Tel: +964 790 144 9044; E-mail: r_awsy@yahoo.com

Received date: November 08, 2018; **Accepted date:** November 22, 2018; **Published date:** November 28, 2018

Abstract

The iron oxide nanoparticles type hematite (α-Fe_2O_3) have been prepared by Sol-Gel technique using ferric nitrate and sodium bicarbonate as precursors. The products were annealing at (200, 300, 400 and 500°C) and characterized by X-ray diffraction (XRD), atomic force microscopy (AFM), surface morphology by scanning electron microscopy (SEM) and fourier transform infrared spectroscopy (FTIR) spectrum. The results showed that the product was α-Fe_2O_3 nanoparticles, and the increasing temperature was an important factor in the formation of α-Fe_2O_3 nanoparticles. The average grain size found to be (79.715 -11.311 nm) after annealing between (200 -500°C).

Keywords: X-ray diffraction; Morphology; α-Fe_2O_3

Abbreviations: α-Fe_2O_3: Hematite alpha iron oxide; γ-Fe_2O_3: Gama iron oxide; XRD: X-ray diffraction; AFM: Atomic force microscopy; SEM: Scanning electron microscopy; FTIR: Fourier transforms infrared spectroscopy; Fe $(NO_3)_3.9H_2O$: Ferric nitrate nonahydrate; $NaHCO_3$: Sodium bicarbonate.

Introduction

There is great interest in the preparation of transition metal oxide nanoparticles as a result of their finding of extensive use in catalysis [1], for solar energy conversion [2] and in the preparation of ferrofluids [3]. Nanometal oxide materials are a new class of materials which provide one of the greatest potentials for improving the performance and extending their applications in various fields of material sciences and technology, as well as biomedical sciences [4-6]. Among these iron oxides, α-Fe_2O_3 (Hematite), has been extensively studied which is the most stable iron oxide with n-type, a hexagonal structure, exhibit paramagnetic behavior and semiconducting properties under ambient conditions, Hematite is the most researched and most frequently polymorphed in nature and its wide technological importance in pigments, catalysis, electrode materials, strong catalytic activity, widely and easily available, and are extremely environment friendly. Hematite may be a promising candidate for visible-light photocatalysis it can absorb visible light, gas sensors [7] and is one of the cheapest semiconductor materials available [8-10], because of its low cost, high resistance to corrosion and environmentally friendly properties. α-Fe_2O_3 nanoparticles have been produced through different synthetic methods [11,12], these methods of synthesis particles have been elaborated such as the sol-gel [13], microemulsion [14], sonochemical [15] microwave plasma [16]. It was observed that the nanoparticles manifested very different physical and chemical properties depending on their microstructure, such as size uniformity and crystallinity. Therefore, developing a synthesis method that can maintain size uniformity and crystallinity is critical for the application of these nanoparticles [17]. The modification of sol-gel technology is a promising approach to obtain advanced metal oxide materials [18,19]. This variation of the sol-gel technology allows the preparation of nanomaterials in forms of sol, powder, film and ceramics. It is based on the precipitation of metal hydroxides and consecutive transformation of the precipitate into sol, gel and crystalline oxide [20].

In this work α-Fe_2O_3 nanoparticles was prepared by the sol-gel method using iron nitrate and sodium bicarbonate as precursor. The α-Fe_2O_3 was annealed at four different temperatures to prepare nanocrystalline powder with different particle sizes. The nanocrystallites were examined by X-ray diffraction (XRD), atomic force microscope (AFM), scan electronic microscope (SEM) and FTIR spectroscopy measurements.

Experimental

Ferric nitrate ($Fe(NO_3)_3.9H_2O$), sodium bicarbonate ($NaHCO_3$), ethanol (C_2H_6O) were of AR grade and were used as received without further purification. In a typical experiment, the α-Fe_2O_3 nanoparticles were prepared by dissolving 10 g of ferric nitrate in a 100 ml of deionized water in baker (500 ml) and move it for 15 minutes at room temperature by the magnetic stirrer to ensure all the salt is dissolved and the solution is quite clear. Dissolving 6.2376 g of sodium bicarbonate ($NaHCO_3$) in 40 ml of deionized in baker (100 ml) and move it to a period of 15 minutes at room temperature by magnetic stirrer to ensure all the base granules are dissolved and the solution is completely clear and then transferred to a volumetric flask (50 ml) and complements the volume to the mark3 Put first solution (ferric nitrate solution) on a magnetic stirrer and start of the magnetic engine running, and placed a second solution (sodium bicarbonate solution) in the burette. Dropping burette solution to the first solution drop by drop (2-3) drops/min with continued stir. Brown precipitate begins to happen with every addition to the base and checks the pH solution (by litmus paper) until the arrival of the pH to 8, where the interaction is complete. The precipitate is separated from the solution and washed

with distilled water several times until the washing solution becomes neutral. After that the precipitate wash (2-3) times with ethanol then separated by centrifuge. Dried the precipitate then use electric furnace at a temperature of 100°C, the precipitate was brown-red powder, the percentage of the product is 75%. The following equations show how the transformation of ferric nitrate to ferric hydroxide and ultimately into ferric oxide.

$2Fe(NO_3)_3.9H_2O+6NaHCO_3=2Fe(OH)_3+6NaNO_3+6CO_2+18H_2O$ (1)

$2Fe(OH)_3=Fe_2O_3+_3H_2O$ (2)

The final equation is:

$2Fe(NO_3)_3.9H_2O+6NaHCO_3=Fe_2O_3+6NaNO_3+6CO_2+2H_2O$ (3)

Annealing treatments for ferric oxide (Fe_2O_3)

Dissolved part of the brown-red powder precipitate in 5 ml of ethanol and put on the heating plate magnetic stirrer 40°C for 90 minutes. Take a quartz slide and immerse in Fe_2O_3 solution for a minute and dried quartz slide repeat this process several times (7-9) in order to be a homogeneous layer on the slide 3 Powder ferric oxide annealing by heating in a furnace at different temperatures of (200, 300, 400, and 500°C) for 90 min, by refractory ceramic crucible.

X-Ray Diffraction (XRD)

The structure of the ferric oxide powder was studied by Xray diffract meter using CuKα radiation (λ=1.54050 A). XRD spectra of the powder were recorded by scanning 2θ in the range (20-80) deg. X-ray diffraction measurement has been done and compared with the Joint Committee on Powder Diffraction Standards (JCPDS) cards.

Fourier Transforms Infrared Spectroscopy (FT-IR):

The infrared spectra of the prepared for ferric oxide nanoparticles with KBr disc were recorded using: FT-IR 8400 S Shimadzu in the range of 4000-200 cm^{-1} at 25°C.

Atomic Force Microscope (AFM)

Ferric oxide nanoparticles were measured using atomic force microscopy. (AFM) using a scanning probe microscopy (CSPM-5000) instrument.

Scanning Electron Microscopy (SEM)

Morphology studies of ferric oxide nanoparticles were carried out with a scanning electron microscope (SEM) type VEGA TE SCAN, with an accelerating voltage of 30 kV and magnification of 10000x.

Results and Discussion

Characterization of nanoparticles

The XRD is employed for the identification and understanding the crystalline growth nature of α-Fe_2O_3 nanoparticles prepared by sol-gel method. The synthesized product of α-Fe_2O_3 was examined by X-ray diffraction (XRD) pattern. The XRD of the nanoparticles are shown in Figures 1a-1d. All these peaks were successfully assigned and indexed in the figure considering a rhombohedral unit cell of standard JCPDS cards.

The annealing temperature plays an important role in determining the structure of Fe_2O_3 nanoparticles, the X-ray diffraction patterns of Fe_2O_3 nanoparticles show good crystalline as in Figure 1. The diffraction peaks agree with those given in JCPD data card of bulk Fe_2O_3 refraction. Where the reflection peaks at (211), (220), (311), (212), (110) and (440) are belong to γ-Fe_2O_3 and that's at (104), (113) and (024) are belong to α-Fe_2O_3.

High diffraction peaks for Fe_2O_3 at 200°C, showed the presence of both α and γ-phases. The reflection peaks at (211), (220), (311), (212), (110) and (440) are belong to γ-Fe_2O_3 and that's at (104), (113) and (024) are belong to α-Fe_2O_3, as in Figure 1a. On increasing heat treatment temperature at 300°C, the hematite structure evolves along with phases of γ-Fe_2O_3. The X-ray diffraction patterns of Fe_2O_3 nanoparticles show in Figure 1b, the diffraction peaks refractions improved with (012), (104), (110) and anther peaks at (113), (024), (116), (214), (300) and (101). At 300°C temperature, the Fe_2O_3 transformation further proceeds to hematite from γ-Fe_2O_3 to α-Fe_2O_3. Treatment at 400°C, and 500°C the composition Fe_2O_3 remains same with improved of reflection peaks (012), (104), (110), (113), (024), (116), (122), (214), (300) and (101), as hematite α-Fe_2O_3 and after that complete phase transformation of nanoparticles occurred. The diffraction pattern of α-Fe_2O_3 at 400°C and 500°C show in Figures 1c and 1d.

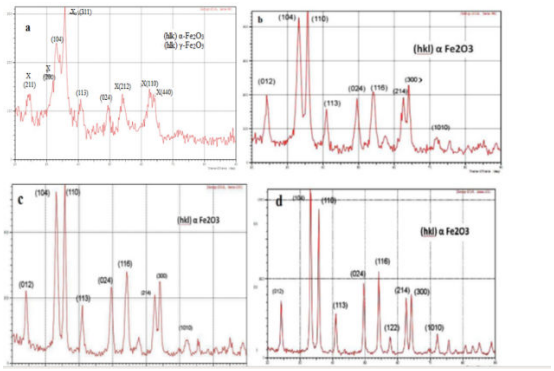

Figure 1: XRD patterns of Fe_2O_3 nanoparticles at different annealing temperatures at: (a) 200°C, (b) 300°C, (c) 400°C and (d) 500°C.

From these figures, it can be seen that there is an increasing in intensity of (104) and (110) orientation, this may be due to heat treatment that enhances the mobility of atoms in rearrangement processes inside the lattice. The heat energy that provided to the atoms could decrease the defect in the Fe_2O_3 nanoparticles and improve quality. This leads to decreases in Full Width at Half Maximums (FWHM) of the reflection peaks which become narrower as the particle size increases, which is a general size-dependent phenomenon within nanoparticles. The mean particle diameter of the Fe_2O_3 was calculated from Debye-Scherer's equation which is given by equation (4) [21,22].

$D=0.9\lambda/\beta \cos\theta$ ……. (4)

Where D is the grain size, λ is the X-ray wavelength, β is the diffraction peak at FWHM, and θ is the diffraction peak position was calculated from the XRD pattern according to the line width of the

(104) plane refraction peak. The lattice constants (a and c) of the Fe_2O_3 powders calculated using the formula in equation (5):

$1/d_2=((h_2+k_2)/a_2)+(l2/c_2)$……..(5)

Where 'd' is the interplanar distance, (h kl) are the Miller indices, 'a' and 'c' is the lattice constants for the tetragonal structure of α-Fe_2O_3. The calculated crystallite size (D) and lattice constant (a and c) of Fe_2O_3 are tabulated in Table 1.

It is observed that the Fe_2O_3 crystallinity improves with increasing substrate temperature (300°C to 500C) for studies peaks (110, 101 and 211) evident from XRD pattern. The crystallite size of Fe_2O_3 obtained using Debye-Scherer's equation and the XRD parameters of nanostructures at various crystalline orientations at 200, 300, 400 and 500°C respectively were shown in Table 1.

Annealing Temperature for 60 min	2θ (deg)	hkl	FWHM (β)(deg)	D Grain Size (nm)	d (nm)	Lattice constant a (Å)	Lattice constant c (Å)
200°C	34.4035	104	5.2391	15.867	26.0468	5.105	13..34
	40.66	311	2.5867	32.7389	22.1716		
	54.243	116	2.7667	32.2495	16.897		
	63.0233	300	3.6	25.8748	14.7377		
300°C	33.2596	104	1.36	60.9432	26.916	5.021	13.708
	35.7363	110	0.8774	95.0993	25.1053		
	54.1239	116	1.2495	71.3682	16.9314		
	64.0782	300	0.7922	118.2631	14.5203		
400°C	33.266	104	1.0138	81.7545	26.911	5.028	13.721
	35.7708	110	0.7487	111.4584	2.50819		
	54.1825	116	1.0601	76.4211	1.69145		
	64.1047	300	0.83	112.8905	1.4515		
500°C	33.2925	104	0.6227	133.1161	2.68901	5.024	13.68
	35.7829	110	0.5697	146.4787	2.50737		
	54.2153	116	0.6167	144.6646	1.6905		

	64.1537	300	0.602	155.6831	1.45051		

Table 1: The obtained result of the XDR for Fe_2O_3 at different annealing temperature (200°C, 300°C, 400°C and 500°C) for 90 min.

It is observed that the Fe_2O_3 prepared at 200°C seems to be less grain size (15.8-32.7) nm. The high-intensity peaks observed with increasing substrate temperature to (500°C) and grain size improves 133.1-155.6 nm. Increasing the annealing temperature leads to increasing grain size, this could be attributed to increasing in the interplanar distance (d) due to excess oxidization process, oxygen atom occupied oxygen vacancies sites which agree with reference [23]. According to equation (2), the lattice constants (a and c) at annealing temperature (300-500°C) were found arriving at 5.02 and 13.7 Å respectively this agree with (JCPDS, Ref. Code: 33-0664).

Effect of annealing temperature on FT-IR

The FT-IR spectra of Fe_2O_3 nanoparticles synthesized at the optimized preparation conditions and at different annealing temperatures are shown in Figure 2.

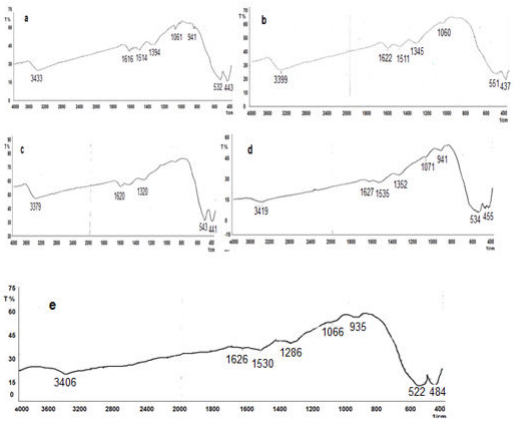

Figure 2: FT-IR transmittance spectrum of Fe_2O_3 (a) as-prepared, annealing at (b) 200°C, (c) 300°C, (d) 400°C and (e) 500°C as the function of wave number.

The most prominent absorption bands detected after thermal annealing are quite similar, with the main absorption bands (around 3433 cm^{-1}) due to water and low wave number bands around 1620 cm^{-1}) these bands are characteristic of stretching and bending of O-H bond respectively [24]. The other bands between (532-522 and 484-434) cm^{-1} due to vibration of the Fe-O bond [25]. The effect of different annealing at (200, 300, 400 and 500°C) show clear decrease the band at 3433 cm^{-1} with the increase of annealing temperature this result due to loss of water molecules in samples. In the same time the Fe-O, bonding more appeared as shown in Figures 2d and 2e. These results are summarized in Table 2.

Fe_2O_3	(O-H) str.[a]	(O-H) ben.[b]	(Fe-O) asym.[c]	(Fe-O) sym.[d]
As-prepared	3433	1616	532	443
200°C	3379	1622	551	437
300°C	3379	1620	543	441
400°C	3419	1627	534	455
500°C	3406	1626	522	484

Table 2: Absorption bands (cm^{-1}) in the FT-IR spectrum of the Fe_2O_3 as prepared and annealing nanoparticles indicates as [a]Stretching, [b]bending, [c]asymmetric, [d]symmetric.

Morphology of Fe_2O_3 nanoparticles

Surface morphology atomic force microscopic (AFM): The surface morphology of Fe_2O_3 nanoparticles was analyzed using atomic force microscope. Figure 3 show a typical two- and three-dimensional AFM image of Fe_2O_3 nanoparticles with annealing at (200°C, 300°C, 400°C and 500°C). The average grain size found to be 75.92 nm when annealing at 200°C (Figure 3).

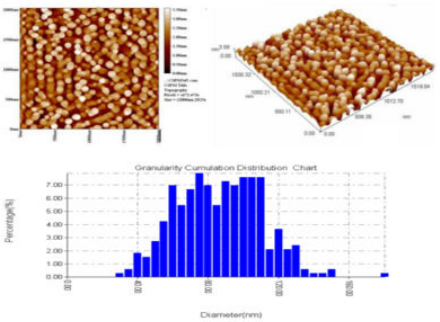

Figure 3: 2 and 3-D AFM image for α-Fe_2O_3 after annealing at 200°C.

While Figure 4 shows the average grain size that annealing at 300°C was 83.51 nm. The AFM results show that the grain size increase by increasing temperature this is due to improving the crystalline of the particles. Figure 5 show the granularity accumulation distribution chart of Fe_2O_3 with annealing at 400°C, and 500°C. The average grain size found to be (89.20 nm -97.61 nm) respectively (Figure 6).

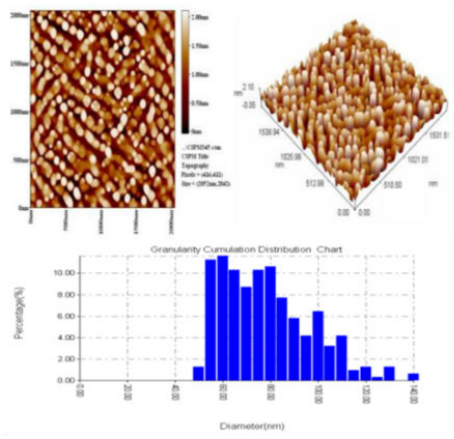

Figure 4: 2 and 3-D AFM image for α-Fe_2O_3 after annealing at 300°C.

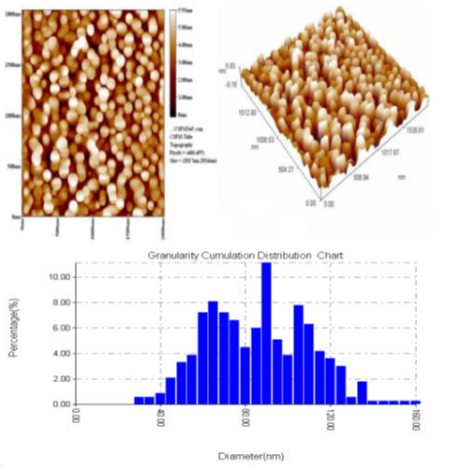

Figure 5: 2 and 3-D AFM image for α-Fe_2O_3 after annealing at 400°C.

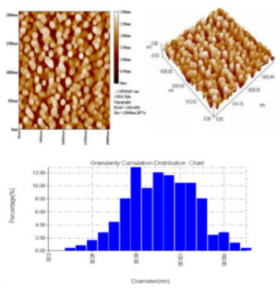

Figure 6: 2 and 3-D AFM image for α-Fe_2O_3 after annealing at 500°C.

Surface morphology by (SEM): The SEM micrographs of the as-prepared powder and samples annealed at 300°C are shown in Figure 4. As seen, nanoparticles have been grown as individual clusters with few agglomerates over the surface. Particles sintered at a lower temperature composed of many particulates with smaller sizes with average gran size 91 nm, as shows in Figure 7a. On the other hand, particles sintered at higher temperature composed of a smaller number of particulates with larger sizes; this was due to the growth and combination of small grains together after sintering process, with average gran size 120 nm, as shows in as in Figure 7b.

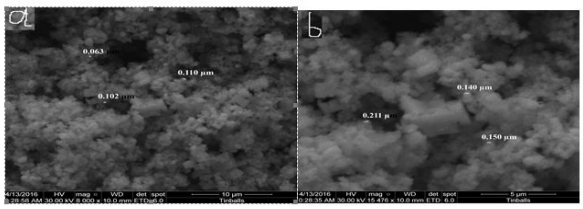

Figure 7: SEM image for Fe_2O_3 thin films (a) as-prepared and (b) annealed at 300C.

Conclusion

The XRD result reveals that Fe_2O_3 nanoparticles have good crystalline as they prepared and their crystalline increase as they annealed to a higher temperature. It can be observed that Fe_2O_3 nanoparticles exhibit a polycrystalline having (104), (110) and (111) plans of high peak intensities. The Fe_2O_3 transformation further proceeds to hematite from γ-Fe_2O_3 to α-Fe_2O_3. Treatment at (400°C) and (500°C) the composition Fe_2O_3 remains same as hematite α-Fe_2O_3 and after that complete phase transformation of nanoparticles occurred. The average grain size found to be (79.715 - 11.311 nm) for Fe_2O_3 after annealing between (200-500°C).

Acknowledgments

The authors would like to thank the University of Technology, Applied Sciences Department for technical assistance to complete this work.

References

1. White RL, Newt RMH, Pease RFW (1997) Patterned media: a viable route to 50 Gbit/in2 and up for magnetic recording. IEEE Trans Magn 33: 990-995.
2. Cherepy NJ, Liston DB, Lovejoy JA, Deng H, Zhang JZ (1998) Ultrafast studies of photoexcited electron dynamics in γ- and α-Fe2O3 semiconductor nanoparticles. J Phys Chem B 102: 770-776.
3. Kang YS, Risbud S, Rabolt JF, Stroeve P (1996) Synthesis and characterization of nanometer-size Fe3O4 and γ-Fe2O3 particles. Chem Mater 8: 2209-2211.
4. Yogeswaran U, Chen SM (2008) Recent trends in the application of carbon nanotubes-polymer composite modified electrodes for biosensors: A review. Anal Lett 41: 210-243.
5. Zhang L, Webster TJ (2009) Nanotechnology and nanomaterials: Promises for improved tissue regeneration. Nanotoday 4: 66-80.
6. Engel E, Michiardi A, Navarro M, Lacroix D, Planell JA (2008) Nanotechnology in regenerative medicine: the materials side. Trends Biotechnol 26: 39-47.
7. Gondal MA, Hameed A, Yamani ZH, Suwaiyan A (2004) Laser-induced photocatalytic oxidation/splitting of water over α-Fe2O3, WO3, TiO2 and NiO catalysts: activity comparison. Chem Phys Lett 385: 111-115.

8. Joya MR, Bar´on-Jaimez J, Barba-Ortega J (2013) Preparation and characterization of Fe2O3 nanoparticles. J Phys Confer Ser 466: 1-4.
9. Liu Y, Yu L, Hu Y, Guo C, Zhang F, et al. (2012) A magnetically separable photocatalyst based on nest-like γ-Fe_2O_3/ZnO double-shelled hollow structures with enhanced photocatalytic activity. Nanoscale 4: 183-187.
10. Fu Y, Chen J, Zhang H (2001) Synthesis of Fe2O3 nanowires by oxidation of iron. Chem Phys Lett 350: 491-494.
11. Chen J, Xu L, Li W, Gou X (2005) α-Fe2O3 nanotubes in gas sensor and lithium-ion battery applications. Adv Mater 17: 582-586.
12. Wen X, Wang S, Ding, Y, Wang ZL, Yang S (2005) Controlled growth of large-area, uniform, vertically aligned arrays of r-Fe2O3 nanobelts and nanowires. J Phys Chem B 109: 215-220.
13. Woo K, Lee HJ, Ahn JP, Park YS (2003) Sol-gel mediated synthesis of Fe2O3 nanorods. Adv Mater 15: 1761-1767.
14. Xu H, Cui L, Tong N, Gu H (2006) Development of high magnetization Fe3O4/Polystyrene/Silica nanospheres via combined miniemulsion/emulsion polymerization. J Am Chem Soc 128: 15582-15583.
15. Vijayakumar R, Koltypin Y, Felner I, Gedanken A (2000) Sonochemical synthesis and characterization of pure nanometer-sized Fe3O4 particles. Mater Sci Eng A 286: 101-105.
16. Shou-Zhe L, Hong YC, Uhm HS, Zhe-Kui L (2004) Synthesis of nancrystalline iron oxide particles by microwave plasma jet at atmospheric pressure. J Appl Phys 43: 7714-7717.
17. Cai R, Xue-Hua L, Lei S, Yi-Qian W, Yuan L, et al. (2013) A new modulated structure in α-Fe2O3 nanowires. Chin Physics B 22: 107401-107404.
18. Ivanovskaya M, Bogdanov P, Orlik D, Gurlo A (1999) Gas-sensitive properties of metal oxide sensors prepared by sol-gel technique. Proc VI NEXUSPAN Workshop, Kaunas, Lithuania, pp: 2529-2532.
19. Kotsikau D, Ivanovskaya M (2011) Advanced metaloxide nanomaterials for gas sensors with controlled properties. Sci Technol Sci 1: 1-6.
20. Brinker JC and George SW (2013) Sol-gel science: the physics and chemistry of sol-gel processing. Academic press.
21. Cornell RM, Schwertmann U (1996) The iron oxides: structure, properties, reactions, occurrence and uses, pp: 533-559.
22. Rasheed RT, Al-Algawi SD (2016) Annealing effect of SnO2 nanoparticles prepared by the sol-gel method. J Adv Phys 5: 236-240.
23. Abdulkadir I, Aliyu AB (2013) Some wet routes for synthesis of hematite nanostructures. Afr J Pure Appl Chem 7: 114-121.
24. Rao CNR (1963) Chemical applications of infrared spectroscopy. New York and London: Academic Press 144: 1441.
25. Basavaraja S, Balaji DS, Bedre MD, Raghunandan D, Prithviraj Swamy PM, et al. (2011) Solvothermal synthesis and characterization of acicular α-Fe2O3 nanoparticles. Bull Mater Sci 34: 1313-1317.